Title

Characterization of microseismic source mechanism in the Marcellus shale through analysis in the spectral domain

Permalink

https://escholarship.org/uc/item/5dx443h1

Authors

Nava*, Michael J
Rector, James W
Zhang, Zhishuai

Peer reviewed

Characterization of Chromium Bioremediation Products in Flow-Through Column Sediments Using Micro–X-ray Fluorescence and X-ray Absorption Spectroscopy

1.   **Charuleka Varadharajan** [*a],
2.   **Ruyang Han**[ab],
3.   **Harry R. Beller**[a],
4.   **Li Yang**[a],
5.   **Matthew A. Marcus**[c],
6.   **Marc Michel**[d] and
7.   **Peter S. Nico**[a]

[+] Author Affiliations

Abstract

Microbially mediated reductive immobilization of chromium is a possible remediation technique for sites contaminated with Cr(VI). This study is part of a broader effort investigating the biogeochemical mechanisms for Cr(VI) reduction in Hanford 100H aquifer sediments using flow-through laboratory columns. It had previously been shown that reduced chromium in the solid phase was in the form of freshly precipitated mixed-phase Cr(III)-Fe(III) (hydr)oxides, irrespective of the biogeochemical conditions in the columns. In this study, the reduced Cr phases in the columns were investigated further using spectroscopy to understand the structure and mechanisms involved in the formation of the end products. Several samples representing potential processes that could be occurring in the columns were synthesized in the laboratory and characterized using X-ray absorption near edge structure (XANES) and X-ray scattering. The XANES of Cr(III) particles in the columns most closely resembled those from synthetic samples produced by the abiotic reaction of Cr(VI) with microbially reduced Fe(II). Microbially mediated Cr-Fe reduction products were distinct from abiotic Cr-Fe (hydr)oxides [$Cr_xFe_{1-x}(OH)_3$] and organically complexed Cr(III) sorbed onto the surface of a mixed ferrihydrite-goethite mineral phase. Furthermore, analyses of the abiotically synthesized samples revealed that even the end products of purely abiotic, iron-mediated reduction of Cr(VI) are affected by factors such as the presence of excess aqueous Fe(II) and cellular matter. These results suggest that $Cr_xFe_{1-x}(OH)_3$ phases made under realistic subsurface conditions or in biotic cultures are structurally different from pure $Cr(OH)_3$ or laboratory-synthesized $Cr_xFe_{1-x}(OH)_3$. The observed structural differences imply that the reactivity and stability of biogenic $Cr_xFe_{1-x}(OH)_3$ could potentially be different from that of abiotic $Cr_xFe_{1-x}(OH)_3$.

Abbreviations

ALS, advanced light source; PCA, principal component analysis; PDF, pair distribution function; XANES, X-ray absorption near edge structure; XRD, X-ray diffraction; XRF, X-ray fluorescence

Chromium is used in several industrial processes and is a common pollutant in groundwater and soils. The remediation of chromium contamination typically involves reducing the toxic and soluble hexavalent form, Cr(VI), to the relatively harmless and mostly immobile trivalent state, Cr(III), through chemical or biological methods. Typical reductants include ferrous iron, either in solution or present as Fe(II)-bearing minerals (e.g., Eary and Rai, 1988; Fendorf and Li, 1996; Sedlak and Chan, 1997); zerovalent Fe (Manning et al., 2007); reduced S compounds (Patterson et al., 1997); and soil organic matter (Jardine et al., 1999). Direct enzymatic reduction of Cr(VI) by microbes has also been suggested as an alternate remediation mechanism (e.g., Arias and Tebo, 2003). The effectiveness of the treatment processes depends on the rate of reduction and the stability of the reduced products (Palmer and Wittbrodt, 1991).

The abiotic reduction of Cr(VI) by aqueous Fe(II) occurs rapidly and results in the formation of $Cr_{0.25}Fe_{0.75}(OH)_3$ (Eary and Rai, 1988). The indirect reduction of Cr(VI) by biogenic Fe(II) also occurs quickly, resulting in a mixed-phase Cr-Fe (hydr)oxide, typically of the form $Cr_xFe_{1-x}(OH)_3 \cdot nH_2O$, where the Cr:Fe ratio will depend on whether the products are further reduced by Fe-reducing bacteria (Wielinga et al., 2001; Hansel et al., 2003; Whittleston et al., 2011). In contrast, direct enzymatic reduction of Cr(VI) is thought to produce Cr(III) (hydr)oxide precipitates or organically complexed Cr(III) that can be bound to cell surfaces or dissolved in solution (Neal et al., 2002; Puzon et al., 2005; Han et al., 2010). The solubility and potential for reoxidation by oxidants will depend on the final structure of the end product(s) (Dai et al., 2009). In general, the solubility of the mixed Cr-Fe solids increases with increasing Cr content, although pure $Cr(OH)_3$ is relatively insoluble (Sass and Rai, 1987).

We present results from spectroscopic and X-ray scattering analyses of the end products derived from microbially mediated Cr(VI) reduction that had been observed previously as part of a broader experiment with flow-through laboratory columns containing sediments from the Hanford 100H aquifer. An overview of the experiment and integrated results and discussion from geochemical, microbial, and spectroscopic analyses of the columns are presented in Beller et al. (2014). Briefly, Beller et al. (2014) investigated the biogeochemical mechanisms for chromium reduction in flow-through columns by exposing them to anaerobic, synthetic groundwater containing Cr(VI) and lactate in the presence of different electron acceptors [SO_4^{2-}, NO_3^-, and Fe(III)]. They observed divergent biogeochemical conditions in the columns, including fermenting conditions and rapid Cr(VI) reduction in some of the columns to which sulfate had been added, as well as denitrification and active Cr(VI) reduction in all the columns containing nitrate. The columns to which no external electron acceptor had been added [i.e., native Fe(III) minerals were the main electron acceptor] had the least amount of Cr(VI) and lactate consumption.

The authors concluded that the reduced Cr products in the columns were present as mixed-phase Cr(III)-Fe(III) (hydr)oxides despite differences in the prevailing biogeochemical conditions after treatment. It was hypothesized that Fe, the electron acceptor present in the native sediments of all the columns, likely played an important role in the reductive precipitation of Cr in the columns. Possible mechanisms included Fe(II)-mediated reduction and/or nucleation of reduced Cr-rich precipitates onto Fe-(hydr)oxide particles.

In this study, the distribution, composition, and structure of reduced Cr phases in the column sediments were further investigated using micro–X-ray fluorescence (µXRF) mapping, X-ray absorption near edge structure (XANES) spectroscopy, X-ray total scattering, and pair distribution function (PDF) analyses. The XANES spectra of Cr minerals in the columns were compared with laboratory-synthesized samples to understand the structure and mechanisms involved in the formation of the end products.

Materials and Methods

Column Experiment and Solid-Phase Analyses of Sediments

This study was part of a broader flow-through column experiment that has been previously described by Beller et al. (2013, 2014). Briefly, the experiment involved 14 columns made using 6-mL, sterile, solid-phase extraction cartridges packed with homogenized sediments from the Hanford 100H aquifer. The columns had been continuously exposed to anaerobic, synthetic groundwater containing Cr(VI), lactate, and different electron acceptors for ~300 d at 3 µL min^{-1} in an upflow (bottom-up) mode. The synthetic groundwater contained 5 µmol L^{-1} Cr(VI), 5 mmol L^{-1} sodium lactate, 1.25 mmol L^{-1} sodium bicarbonate, 1 mmol L^{-1} potassium phosphate buffer (pH 7), 1.6 mmol L^{-1} calcium chloride, and 0.1 mmol L^{-1} ammonium chloride. Additional electron acceptors had been added to some of the columns as shown in Table 1. The columns had been stored in an anaerobic glovebox with an ultra–high purity N$_2$ atmosphere.

View Full Table | Close Full View Table 1.

Overview of conditions in laboratory flow-through columns.†

Name	Electron acceptor added	No. of columns
(Sulfate-amended) fermenting	sulfate (7.5 mmol L^{-1} MgSO$_4$)	2
	sulfate	
Sulfate-amended low activity	sulfate (7.5 mmol L^{-1} MgSO$_4$)	4
(Nitrate-amended) denitrifying	nitrate (12 mmol L^{-1} KNO$_3$)	5
No electron acceptor added; low activity	no external acceptor added (native Fe minerals)	3

[†]Experimental setup in Beller et al. (2013, 2014).
[‡]From Supplemental Table S1.
[§]Firmicute *Pelosinus* sp. strain HCF1 capable of fermentation and enzymatic reduction of Fe(III) and Cr(VI).
[¶]Proteobacteria potentially capable of enzymatic Cr reduction.

For this study, four columns representing the dominant biogeochemical characteristics that had been prevalent through the broader experiment (i.e., sulfate-amended fermenting, sulfate-amended low-activity, nitrate-amended denitrifying, and no added electron acceptor low-activity columns) were destructively harvested for solid-phase analysis and for comparison with native, untreated Hanford 100H sediments. Each column was sectioned lengthwise into three approximately equal portions. Extractable Cr and Fe in the different sections and untreated sediments were measured by adding 10 mL of 0.5 mol L^{-1} HCl to 0.5 g of air-dried sediment for 1 h in a glove box (Lovley and Phillips, 1987). Total Cr and Fe concentrations were determined using ICP–MS (PerkinElmer SCIEX ICP-Mass Spectrometer ELAN DRC II), and Fe(II) was measured colorimetrically with ferrozine (Stookey, 1970). A small sample of sediment was taken from the bottom section of each column, sprinkled on Kapton tape, and mounted on Al sample holders for spectroscopic analysis.

Synthetic Sample Preparation

Several samples were synthesized in the laboratory to understand the mechanism(s) involved in Cr(VI) reduction in the columns. The samples represented various processes that could potentially be occurring in the columns, and a subset was selected as fitting standards for analysis of the column minerals (Table 2). Aqueous solutions were prepared with Milli-Q water (Elix 10 UV system, Millipore), and all glassware was acid washed before use.

View Full Table | Close Full View **Table 2.**

Synthetic samples used to characterize the secondary Cr minerals present in the columns. Samples that were selected as fitting standards for the column minerals are highlighted as bold text.

Sample	Method of preparation
Microbially mediated samples	
Pellet 1	Cr(VI) + lactate + HCF1†
Pellet 2	Fe(III)-NTA‡ + lactate + HCF1
Pellet 3¶	**Cr(VI) + Fe(III)-NTA + lactate + HCF1**
Pellet 4	step 1: Fe(III)-NTA + lactate + HCF1 incubated overnight at 30°C; step 2: Heat cel 80°C to denature enzymes; step 3: Add Cr(VI)
Pellet 5	steps 1 and 2 same as for pellet 4; spin down cells, resuspend in fresh medium, a
Abiotic Cr-Fe samples	
Cr$_{0.1}$Fe$_{0.9}$(OH)$_3$	**hydrolysis**
Cr$_{0.25}$Fe$_{0.75}$(OH)$_3$	**hydrolysis**
Cr$_{0.5}$Fe$_{0.5}$(OH)$_3$	**hydrolysis**
Cr$_{0.75}$Fe$_{0.25}$(OH)$_3$	hydrolysis
Cr$_{0.9}$Fe$_{0.1}$(OH)$_3$	hydrolysis
Reduction 1:2.7	Cr(VI) + Fe(II), 1:2.7
Reduction 1:5	**Cr (VI) + Fe(II), 1:5**

Sample	Method of preparation
Reduction 1:40	**Cr (VI) + Fe(II), 1:40**
Reduction 1:5 with heat-inactivated cells	Fe(II) incubated overnight with heat-inactivated cells. Added Cr(VI); Cr:Fe = 1:5
Reduction 1:40 with heat-inactivated cells	Fe(II) incubated overnight with heat-inactivated cells. Added Cr(VI); Cr:Fe = 1:40
Sorption sample	FeOOH added to dissolved Cr-oxalate
Other standards	
Cr(OH)$_3$§	
Cr-oxalate	**purchased reagent**
Cr(VI)§	

†Firmicute *Pelosinus* sp. strain HCF1.

‡NTA, nitrilotriacetic acid.

§Standards not prepared in the laboratory. The XANES data were obtained with permission from Werner et al. (2006).

The microbially mediated samples were prepared as described in Beller et al. (2013) in an anaerobic chamber using cell cultures containing HCF1, 20 mmol L^{-1} lactate, 50 µmol L^{-1}Cr(VI), and/or 2 mmol L^{-1} Fe(III)-nitrilotriacetic acid, a soluble Fe(III) organic complex. Solutions were spun down into a single pellet and put onto a plastic slide for drying overnight.

Abiotic Cr-Fe samples were synthesized using two methods. "Coprecipitated samples" were made following the procedure outlined in Hansel et al. (2003) via hydrolysis of 50 mmol L^{-1}Fe(NO$_3$)$_3$ and CrCl$_3$ solutions, mixed in relevant proportions at pH 2, and then adjusted to pH 7 using 0.1 mol L^{-1} NaOH. The Cr and Fe contents of the prepared samples were verified by digesting the crushed solids in ultra–high purity concentrated nitric acid and analyzing the supernatant solutions by ICP–MS (Supplemental Table S1).

"Reduction samples" were prepared in an anaerobic glove box by mixing 50 mmol L^{-1}KCr$_2$O$_7$ and 50 mmol L^{-1} FeCl$_2$.4H$_2$O (pH ~6.7) solutions that were prepared using 50 mmol L^{-1} PIPES buffer and adjusting the final pH to 7 using NaOH. The solutions were mixed in different molar proportions [Cr (VI):Fe(II)– 1:2.7, 1:5, and 1:40] to determine the effects of a varying range of Fe(II) concentrations in solution, given that the stoichiometric ratio needed for Cr(VI) reduction by Fe(II) is 1:3. Changes to the reduction sample spectra due to amorphous cellular matter were examined by preparing additional samples where Cr(VI) was added to Fe(II) solutions that had been allowed to incubate overnight with heat-inactivated cells.

Chromium(III) oxalate hydrate (Great Western Inorganics) was used to obtain XANES representative of organic Cr. A sample representing sorption of organic Cr to an Fe mineral was prepared by adding FeOOH (characterized as a mixture of goethite and ferrihydrite by scattering analysis; Supplemental Fig. S1) to dissolved Cr-oxalate.

Synchrotron Data Collection and Analysis

Data Collection

Micro–X-ray fluorescence (µXRF) maps and micro–X-ray absorption near edge structure (µXANES) spectra of column sediments were collected at beamline 10.3.2 of the advanced light source (ALS) using a seven-element GE fluorescence detector. The ALS was operating under standard conditions during all the data collection sessions with a ring current of 500 mA in top-off mode.

The µXRF maps were usually collected above the Fe K-edge at 10 keV (or 7.6 keV), with mapping step sizes usually 10 × 10 µm^2 (or 7 × 7 µm^2) and dwell times ranging from 50 to 200 ms per pixel. Fine-scale maps were collected at a mapping step size 1 × 1 µm^2 (X-ray spot size, 2 × 2 µm^2).

Chromium µXANES spectra were collected for energies ranging from ~5.9 to 6.3 keV, with step size ~0.4 eV around the edge. The µXANES spectra were mostly collected in Quick-XAS mode to reduce the potential for beam damage and loss of signal due to sample movement. The µXANES spectra of the coprecipitated samples and the Reduction 1:2.7 sample were collected using a total electron yield device. Powdered samples for total electron yield measurements were smeared onto conductive

carbon tape, and the current was recorded as a function of incident X-ray energy. Kapton polyamide tape was used to cover the rest of the samples to minimize oxidation and to prevent loss of moisture at the beamline. All samples were stored in an anaerobic box before being analyzed at the synchrotron facilities.

Bulk Cr XANES spectra of the column sediments were obtained at beamline 4–1 at the Stanford Synchrotron Radiation Laboratory using a Lytle detector for energies ranging from ~5.8 to 6.3 keV and step size ~0.2 eV around the edge. Individual scans for data collected at the Stanford Synchrotron Radiation Laboratory were averaged in Sixpack (Webb, 2005).

Data Reduction

Data collected at beamline 10.3.2 ALS were first processed using the beamline software. Data reduction and normalization were performed using ATHENA (Ravel and Newville, 2005). Chromium XANES spectra of the synthetic samples were calibrated with the Cr(VI) peak at 5994.5 eV and were aligned using the two pre-edge peaks in the first derivative to account for an ~1.2 eV intra-run beamline calibration shift between column spectra and synthetic samples. Data were normalized using a linear pre-edge from −45 to −15 eV and quadratic post-edge from ~50 to 280 eV. When data quality required modification of these parameters, they were adjusted to minimize differences between normalized spectra to avoid interpreting processing-induced artifacts.

Chromium µXANES Clustering

Chromium µXANES spectra of the column minerals were categorized into groups using hierarchical agglomerative clustering implemented using the statistical software package R (R Core Team, 2013). The metric used to determine the extent of similarity between XANES spectra was the Euclidean distance (i.e., the square root of the sum-squared distances between points corresponding to the same energy values in each spectrum). The linkage criterion used to identify the clusters was the Ward's criterion, which minimizes the variance within a cluster. The tree produced by the clustering algorithm was finally divided into three groups; dividing the tree into additional groups did not change the results or conclusions.

Principal Component and Target Transform Analysis

Principal component analysis (PCA) and target transforms were done in SixPack to identify a set of standards to fit the column minerals from a bigger set of laboratory-synthesized samples. Principal component analysis and target transforms can be used to analyze spectra to identify if they can be represented as linear combinations of a set of standards. The PCA can only identify the number of components that are needed to represent the signal. Further analysis using target transforms can identify the standards that represent each component. A target transform removes all data from a reference spectrum that are not found in the unknown component (Gräfe et al., 2014). The extent to which the reference spectrum is changed by this transformation is indicated using a SPOIL value; SPOIL values <3 are considered good, 3 to 6 are moderately acceptable, and >6 are unacceptable (Malinowski, 2002; Beauchemin et al., 2002). SPOIL values were determined by using the Cr XANES of the samples as target transforms with four components obtained from PCA of the Cr XANES of the secondary minerals.

Linear Combination Fits

Linear combination fitting of Cr XANES spectra was done in Sixpack (Webb, 2005) with a fitting range of 5980 to 6050 eV, positive component weights, and a linear function added to account for normalization differences. The goodness-of-fit was determined using the χ^2 statistic, which is the normalized sum-squared difference between the fit and the XANES spectra at each point in the signal.

First, each synthesized sample was fit using all the other synthetic samples as standards to identify unique samples that could not be represented as a combination of any other materials. Then the column minerals were fit using a subset of the synthetic samples as standards. The final standards used to fit the column minerals (Table 2) were selected based on two criteria: (i) standards that had good or moderately acceptable SPOIL values and (ii) standards that were not a combination of any of the other synthesized materials from the linear combination fits.

X-ray Scattering Data Collection and Analysis

Synchrotron-based X-ray total scattering data were collected at beamline 11-ID-B at the Advanced Photon Source (Argonne National Laboratory). X-ray intensity data were collected using a PerkinElmer amorphous silicon image plate detector. An energy of 58.3 keV (k = 0.2128 Å) was used for wide-angle X-ray measurements, yielding a Q_{max} value of 27 Å^{-1}. The experimental setup was also optimized for the lower-Q region (Q_{max} = 12 Å^{-1}) to obtain conventional-type powder XRD patterns with higher reciprocal-

space resolution. Scattering data on blank samples were measured independently at equal exposure times, allowing for subtraction of parasitic scatter due to the polyimide capillary and water. A CeO_2 standard (NIST diffraction intensity standard set 674a) was used to calibrate the sample-to-detector distance for both experimental setups. Integration of the raw scattering data into spectra was performed with the program Fit2D (Hammersley, 1998), and a polarization correction was applied during the integration procedure.

The program PDFgetX2 (Qiu et al., 2004) was used for data processing of the integrated spectra. The total scattering structure function S(Q) was obtained by normalization according to sample composition (Table 1); the Fourier transform of S(Q), up to a Q_{max} value ranging from 21 to 27 Å^{-1}, yielded the PDF or G(r). The upper limit of the transform was chosen to correspond to the Q value above which the signal-to-noise ratio was close to 1. Standard corrections and corrections typical for the image-plate geometry were applied during data processing (Chupas et al., 2003).

Results

Analyses of Laboratory-Synthesized Samples

Abiotic Cr-Fe Samples

The coprecipitated $Cr_xFe_{(1-x)}(OH)_3$ solid-solution series prepared in the laboratory were the same substances synthesized by Hansel et al. (2003) and Tang et al. (2010), with progressive structural changes observed with increasing Fe content (Fig. 1; Supplemental Fig. S2). Only three out of the five coprecipitated samples were selected as final fitting standards (Table 2). The sample representing sorption (Cr-oxalate + FeOOH) was indistinguishable from the coprecipitated samples based on XANES spectra (Fig. 1) and XRD/PDF analyses (Supplemental Fig. S1) and thus was not included in further data analyses.

Normalized Absorption

Microbially mediated
Pellet 1
Pellet 3
Pellet 4
Pellet 5

Co-precipitation
$Cr_{0.1}Fe_{0.9}$
$Cr_{0.25}Fe_{0.75}$
$Cr_{0.5}Fe_{0.5}$
$Cr_{0.75}Fe_{0.25}$
$Cr_{0.9}Fe_{0.1}$

Reduction
Red. 1:5
Red. 1:5 w/ cells
Red. 1:40
Red. 1:40 w/ cells

Sorption
Cr(III) w/ FeOOH

Other Cr standards
Cr(OH)3

Cr oxalate

Cr(VI)

First Derivative

Fig. 1.
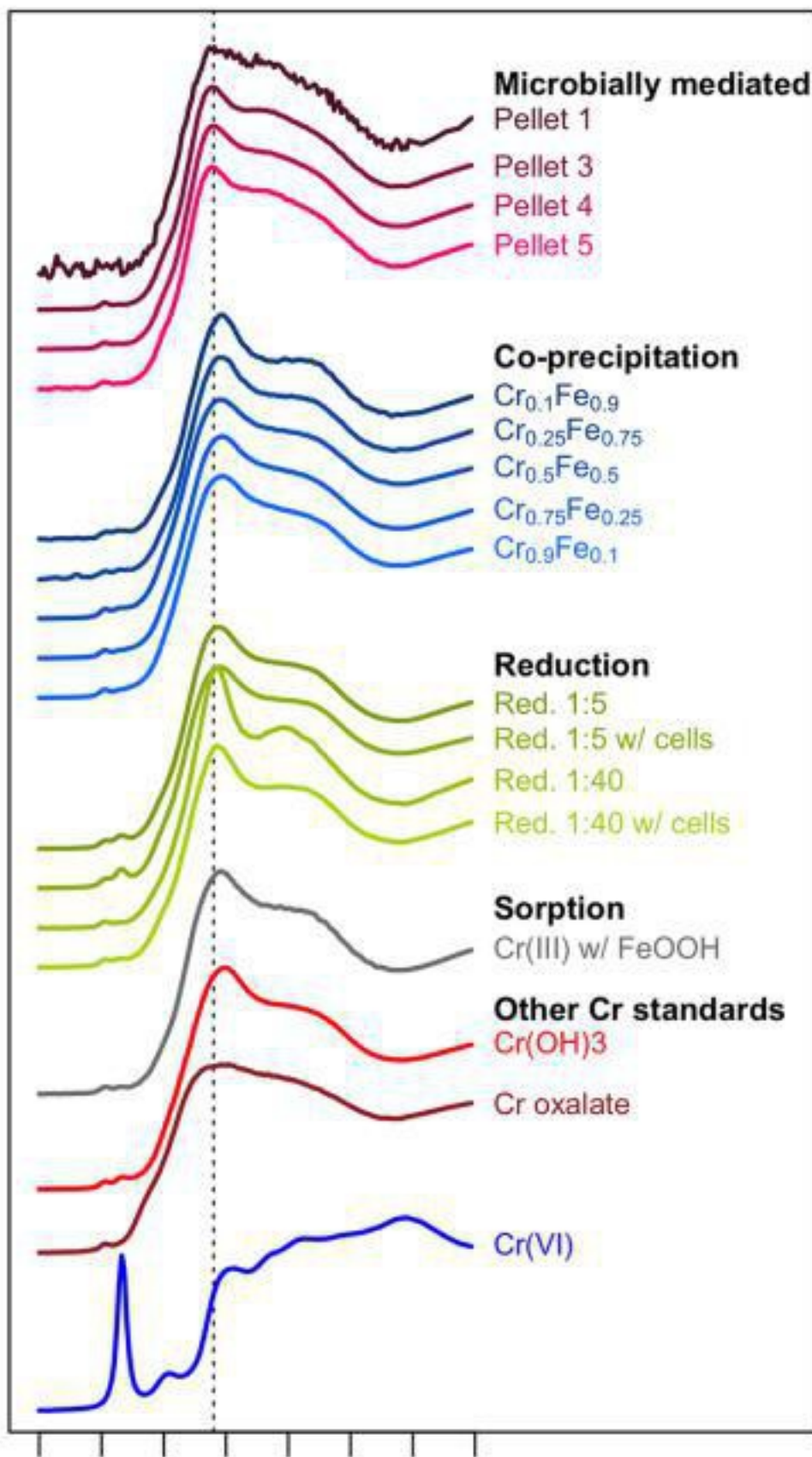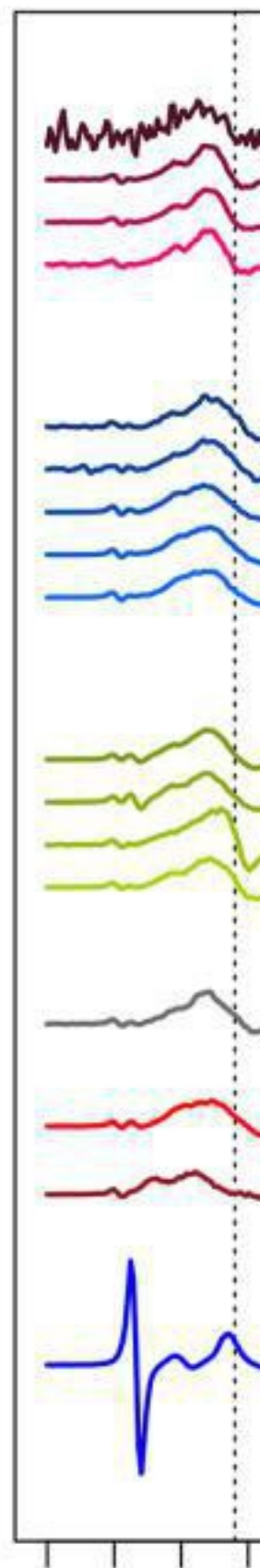
Chromium X-ray absorption near edge structure (XANES) of laboratory-synthesized samples (left) and their first derivatives (right). The dotted guidelines in the panels are shown to visually indicate the difference in peak position between the microbially mediated samples and other abiotic Cr-Fe samples.

The reduction samples with low Fe (Cr:Fe,1:2.7 and 1:5) could not be distinguished from the coprecipitated materials from XANES or from XRD and were thus not used in further data analyses (Fig. 1; Supplemental Fig. S3). In contrast, the reduction sample with high Fe (Cr:Fe, 1:40) was found to be significantly different from all the other samples (Fig. 1) and was thus used as a fitting standard. The addition of cellular matter during the synthesis of the 1:40 reduction sample changed its XANES spectra to be indistinguishable from the spectra of the coprecipitated samples, and hence the sample "Reduction 1:40 with heat-inactivated cells" was not used in the linear combination fits.

Microbial Cell Culture Samples

The microbially mediated samples were different from all the other materials, and their XANES spectra could not be reproduced using any combination of the abiotically synthesized Cr-Fe samples or other Cr materials (Fig. 1). Iron K-edge XANES spectra (data not shown) for these samples were also different from the XANES spectra of abiotic Cr-Fe samples. The sample representing enzymatic Cr reduction (pellet 1) was the most distinct and was noticeably different from pure Cr-oxalate. The fits also revealed that the samples containing Cr and Fe were similar; in fact, pellet 3 (Cr and Fe mixed simultaneously) and pellet 5 [Fe added before Cr; no excess Fe(II)] were almost identical, whereas pellet 4 [Fe added before Cr; excess Fe(II)] was found to be mostly (75–80%) pellet 3 (or 5), with the balance comprising a combination of abiotic Cr-Fe samples.

Chromium Abundance in the Solid Phase of Column Sediments

The 0.5 mol L^{-1} HCl extractions showed that a substantial amount of Cr was sequestered in the solid phase of the treated columns (Table 1; Supplemental Table S2). The maximum amount of extractable Cr was observed in the bottom sections of the fermenting (25.5 ± 0.7 µg $g_{sediment}^{-1}$) and denitrifying (20.7 ± 0.6 µg $g_{sediment}^{-1}$) columns, which were approximately two to four times higher than Cr extracted from the bottom sections of the low-activity columns (Supplemental Table S2). Chromium extracted from the solid phase of the untreated material was very low in comparison to the extractable Cr from the treated columns (0.3 ± 0.1 µg $g_{sediment}^{-1}$ or ~1% of total Cr extracted from the fermenting/denitrifying columns).

Analysis of Cr Minerals in the Column Sediments

X-ray fluorescence microprobe maps from the bottom sections of the four treated columns and the untreated material identified several Cr hotspots (Fig. 2; Supplemental Fig. S4). Micro-XANES spectra were collected from 70 locations in the five samples. Three main groups of Cr particles were identified by hierarchical clustering of the spectra: (i) primary minerals, (ii) chromium metal, and (iii) secondary mineral products (Fig. 3).
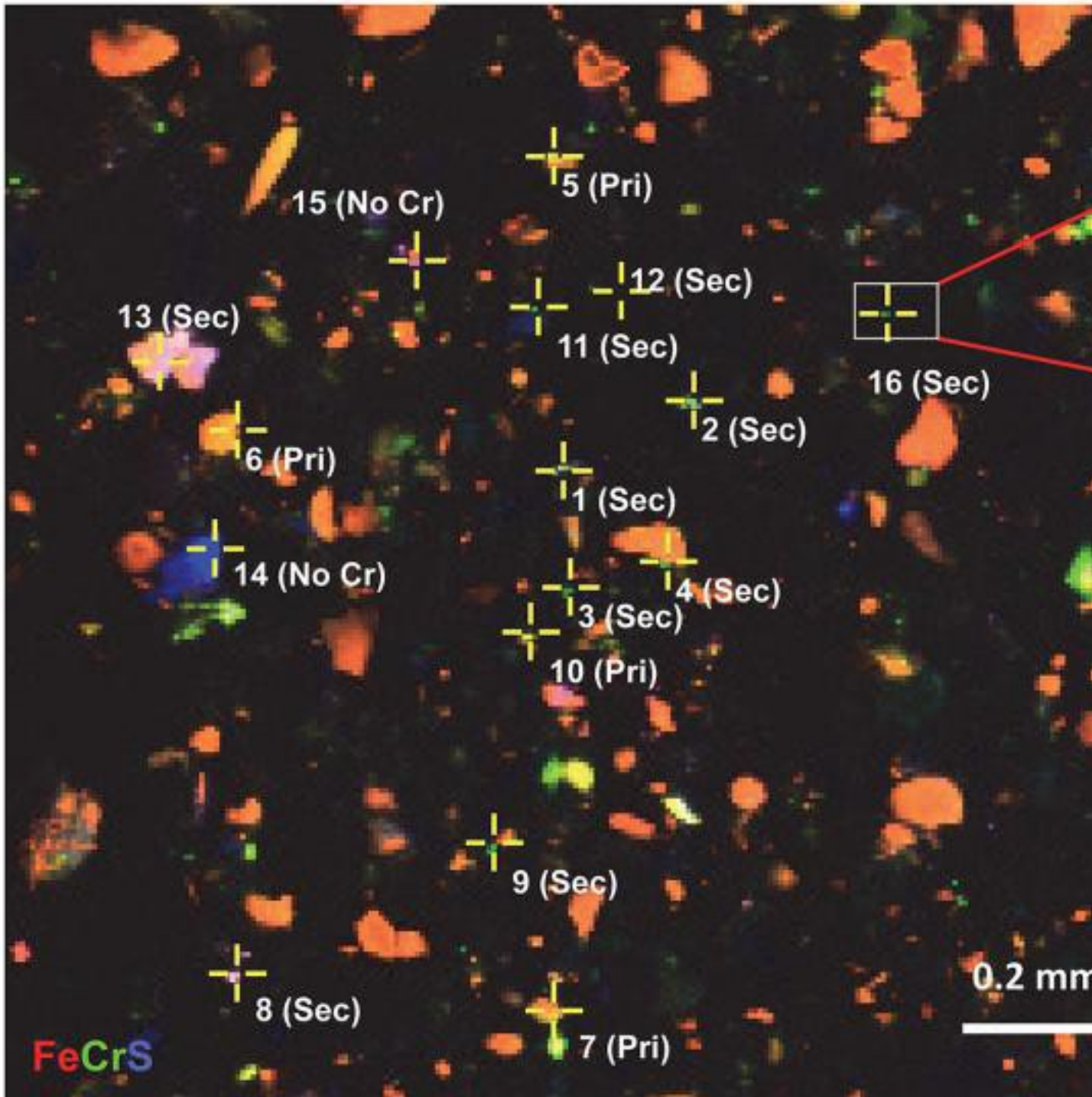
Fig. 2.

Map of the fermenting column (left) showing freshly precipitated Cr-Fe particles (labeled as "Sec") and Cr-bearing primary minerals (labeled as "Pri"). The colors in the map represent Fe (red), Cr (green), and S (blue). A high-resolution map (top right) shows one of the secondary minerals to be ~10 μm in diameter. The ratio of Cr and Fe counts in the fluorescence channels for a cross-section of the particle (indicated by dashed white line) is shown in the bottom right. The Cr and Fe counts were highly correlated (R^2 = 0.8) within the particle.
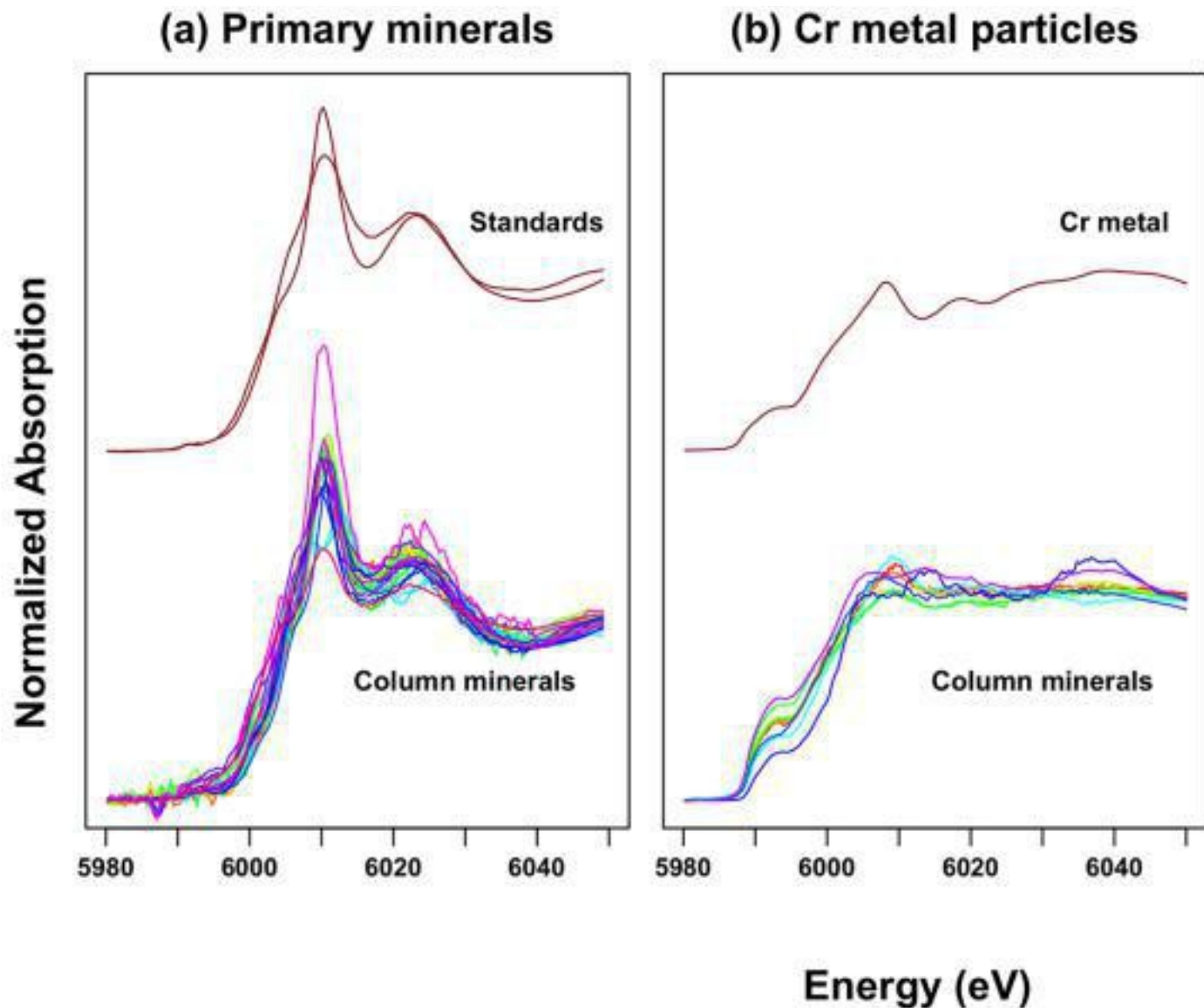
Fig. 3.

Hierarchical clustering identified three groups of Cr X-ray absorption near edge structure spectra (XANES). (a) Primary minerals present in native sediment. The top two spectra are Cr-mica and Cr-spinel shown for reference. (b) Chromium metal of unknown origin. The top spectrum shown for reference is Cr-metal foil. (c) Secondary minerals that are products of treatment. These were found to be very similar irrespective of the prevailing biogeochemical conditions during treatment. Top spectrum shown for reference in the panel is a synthetic Cr-Fe (hydr)oxide [$Cr_{0.25}Fe_{0.75}(OH)_3$] standard.

The first group consists of primary minerals similar to Cr-spinel and mica, which are natively present in the aquifer material (Fig. 3a). The primary minerals were dominant in the untreated sediment and in the low-activity columns where minimal Cr reduction was observed. The second group consists of metal particles of unknown origin (Fig. 3b); their presence also was apparent in the bulk XANES of untreated sediments (Supplemental Fig. S5). The third group consists of a tightly clustered set of secondary mineral products (Fig. 3c) that were far apart from the primary minerals and the metal particles in terms of Euclidean distance (Supplemental Fig. S6). These were only found in the treated columns and were not present in the original, untreated material and hence are also referred to as products of treatment. Visually, the large, bright Cr particles in the μXRF maps were found to be either primary minerals or Cr metal, whereas the small particles were identified as the secondary minerals.

The secondary Cr minerals (products of treatment) were found to be more abundant in the fermenting and denitrifying columns as compared with the low-activity columns. A comparison of Cr bulk XANES and µXANES spectra shows that the dominant form of Cr in the fermenting column changes from primary minerals before treatment to secondary minerals after treatment (Supplemental Fig. S5). Analyses of µXANES spectra from the secondary minerals revealed these to be mixed-phase Cr-Fe (hydr)oxides, $Cr_xFe_{1-x}(OH)_3$ (Fig. 3c) that were very similar to each other, irrespective of the predominant biogeochemical condition during treatment. Some µXANES spectra of the secondary minerals contained a trace Cr(VI) pre-edge peak, indicating incomplete Cr reduction. Fine-scale mapping showed that the secondary mineral products were ~20 µm or less in diameter and were uniformly associated with Fe throughout their cross-section (see Fig. 2), implying that these were small particles (or tight particle clusters that appeared as a single particle within the resolution of the microprobe) rather than coatings.

Comparison of Secondary Cr Mineral Products Found in Treated Column Sediments to Laboratory-Synthesized Samples

Principal Component and Target Transform Analysis

Principal component analysis was performed using 33 secondary mineral µXANES spectra from the four treated columns (Supplemental Table S3). The IND value (Malinowski Indicator value) showed a broad minimum starting with the fourth component. Hence, an additional criterion of decreased marginal improvement in the cumulative variance (i.e., the sum-squared error) was used and also indicated a cutoff at the same component (Gräfe et al., 2014). Based on this, we chose to conduct target transforms using four components that identified several samples as good possible standards (SPOIL <3) and a few as moderately acceptable (SPOIL 3–6) (Table 2). In some cases two components were found to be sufficient; pellets 3, 4, 5 (i.e., the microbially mediated samples containing Cr and Fe) and Cr(VI) were the only ones identified as good standards (SPOIL values 1.2, 1.5, 2.4, and 2.5) with two components.

Linear Combination Fitting

Linear combination fits of column µXANES spectra with selected standards showed that the reduced Cr in the columns was mostly composed of matter resembling the microbially mediated standards containing Cr and Fe(III) (i.e., pellets 3, 4, and 5) (Table 3; Fig. 4). The best fits were obtained with pellet 3 (Cr and Fe mixed simultaneously); χ^2 values for fits using pellets 4 [Fe added before Cr; excess Fe(II)] or 5 [Fe added before Cr; no excess Fe(II)] were slightly higher but still significantly better than fits produced without using the microbially mediated standards as components. Energy shifts for ΔE_0 were small (−0.25 to 0.12 eV), which is within the 0.4 eV step size around the edge. The results were not affected by the introduction of additional constraints, such as setting ΔE_0 shifts to zero or summing components to 1. The accuracy of each fit was assumed to be ~5% (Werner et al., 2006).

View Full Table | Close Full View Table 3.
Linear combination fitting results showing the composition of different components in the secondary mineral precipitates. Also shown are standard deviations for a given component across all spectra within the columns. Propagated errors (χ^2 values) are negligible in comparison to the standard deviations.

Column	No. of spots	Pellet 3	Abiotic Cr-Fe	Cr(VI)	Organic Cr(III)
				%	
Sulfate-amended, fermenting	11	89 ± 6	11 ± 6	0.5 ± 0.7	2 ± 4
Sulfate-amended, low activity	6	77 ± 16	23 ± 16	0.2 ± 0.3	0 ± 0
Nitrate-amended, denitrifying	14	72 ± 17	27 ± 17	0.7 ± 0.9	0 ± 0
No electron acceptor added, low activity	2	54 ± 12	36 ± 15	9.5 ± 2.6	3 ± 4

Fig. **4.**
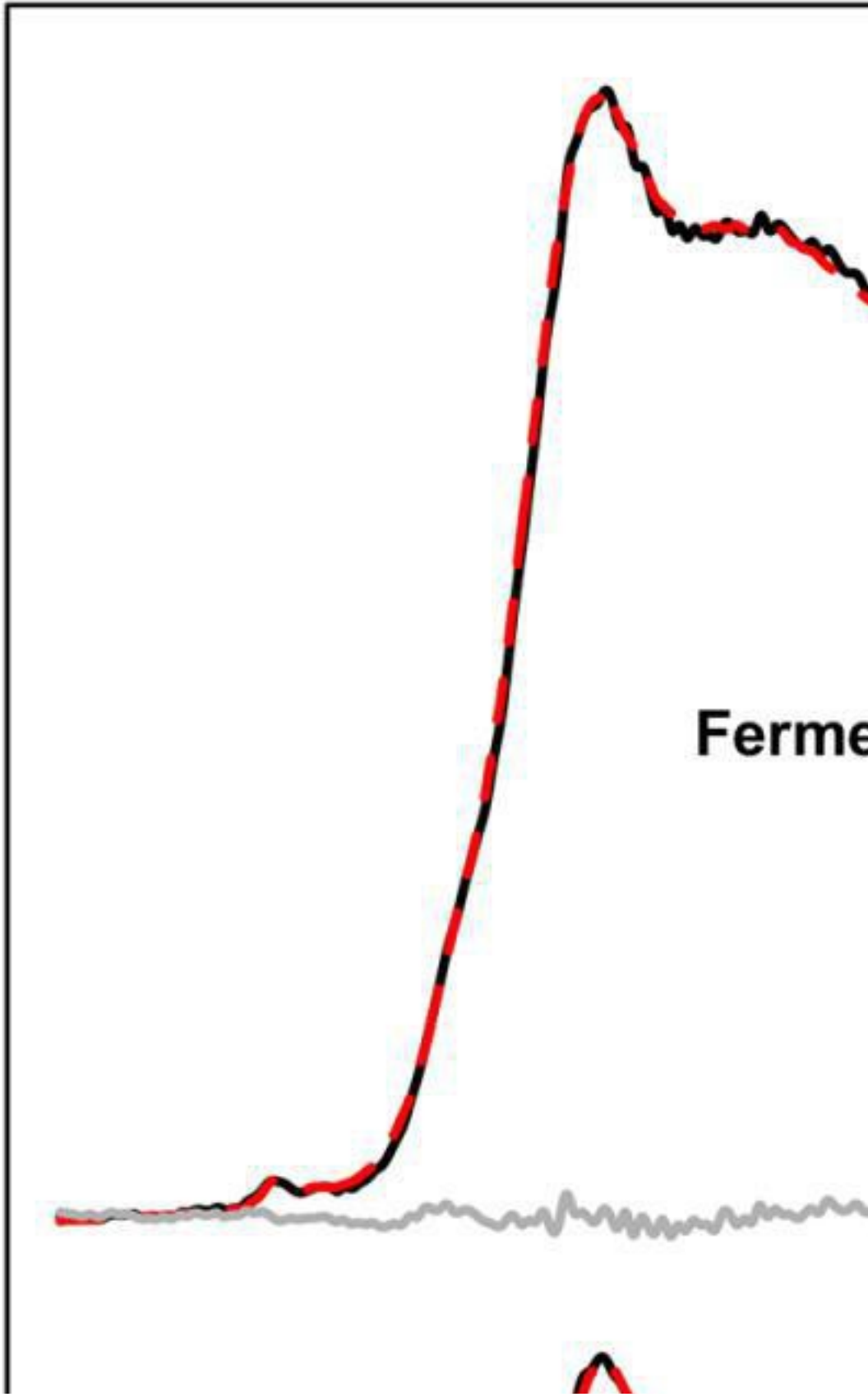
Chromium X-ray absorption near edge structure (XANES) (solid black line), linear combination fits (dotted red line), and residuals (solid gray line) of representative spots from the fermenting and denitrifying columns.

In general, it was not possible to distinguish between different abiotic Cr-Fe materials, despite slight differences among XANES spectra of coprecipitated and reduction standards because several combinations could produce equally good fits. Typically, only the standards with SPOIL values <3 were needed to produce the best fits. Trace amounts of Cr(VI) were found in some spots, particularly in the no-electron-acceptor-added column, indicating incomplete Cr reduction (or possibly reoxidation) (Table 3).

Discussion

Mechanism for Formation of Secondary Minerals

The secondary minerals identified as the fresh products of treatment were the dominant form of Cr in the solid phase of the fermenting and denitrifying columns based on the selective extractions, bulk XANES, and frequency of particles found by micro–X-ray spectroscopy. The secondary minerals in the columns were found to be structurally similar, irrespective of the biogeochemical condition in the column, and clearly distinct from primary minerals or chromium metal.

Comparison of the Cr XANES spectra from the secondary minerals in the columns to the laboratory-synthesized samples shows that these most closely resemble the products of indirect, abiotic reduction of Cr(VI) by biogenic Fe(II) (i.e., pellets 3, 4, and 5). Furthermore, the microbially mediated pellets 3, 4, and 5 were found to be structurally different from Cr reduced by an abiotic source of Fe(II) because (i) they could not be reproduced using a combination of any of the other samples including the coprecipitation, reduction, sorption, or other inorganic/organic Cr samples and (ii) the Cr XANES spectra of the sample containing heat-inactivated cells added to abiotic $Cr_xFe_{1-x}(OH)_3$ were different from the XANES spectra of the pellets. Furthermore, when Cr(III)-oxalate was used to represent organically bound Cr, its addition to FeOOH (characterized as predominantly goethite, with some ferrihydrite) produced a substance resembling the abiotic Cr-Fe samples but not the microbially mediated samples, suggesting that sorption/coprecipitation of organic Cr(III) resulting from enzymatic reduction of Cr(VI) (by fermenting or denitrifying bacteria) onto an Fe mineral was not a viable pathway for the formation of the column materials.

The structural similarity between the secondary Cr(III) minerals found in the columns and the microbially mediated pellets 3, 4, and 5, combined with their structural difference from the end product of Cr reduction by abiotic Fe(II) or surface precipitation/sorption of organically complexed Cr(III) with Fe minerals, suggests that Cr(VI) introduced into the columns was reduced in a manner similar to those mixed biotic–abiotic laboratory samples, specifically the reaction of Cr(VI) with biotically produced Fe(II). The resulting products are structurally different (as determined by XANES) from those generated by any of the other tested formation pathways. There are several possible mechanisms by which this coupled biotic–abiotic pathway may lead to structurally distinct products (as compared with the other synthetic sample), but the two most likely are the rate of reduction, as controlled by Fe(II) concentrations, and the impact of organic ligands/cell surfaces on precipitation morphology and rate. These mechanisms are discussed in more detail below.

Effects of Cellular Matter and Excess Fe(II) on Cr(VI) Reduction

The presence of cellular matter appeared to decrease the amount of Fe(II) available for reduction, as observed in the Cr XANES spectra of synthetic samples. A noticeable Cr(VI) pre-edge peak was observed in the 1:5 reduction sample with cells, possibly indicating incomplete Cr(VI) reduction due to

the decrease in availability of Fe(II). For the reduction sample with high Fe (Cr:Fe, 1:40), complete Cr(VI) reduction was observed with and without cellular matter, but the XANES spectra of the sample with cells had a less definitive shoulder structure compared with the spectra of the reduction 1:40 sample without cells (Fig. 1). One theory to explain the observed spectral differences is that cell surfaces coated with Fe act as "fast precipitation spots" and lead to more abundant nucleation sites and smaller particle sizes. In general, faster precipitation leads to the formation of less-crystalline products (Cornell and Schwertmann, 2003). The structure of the end product could be dependent on the extent of particle nucleation and/or the rate of reduction. Organic/cellular matter is known to serve as preferential sites for nucleation of biomineralization products and can affect the structure of the end phases (Dove et al., 2003).

The presence of excess Fe(II) in solution during the synthesis of the laboratory samples was also found to affect the structure of the Cr-Fe end product. The effect was minor in the microbial cell cultures, as shown by the differences between pellet 4 [Fe added before Cr; excess Fe(II)] and pellet 5 [Fe added before Cr; no excess Fe(II)]. The minor (~20–25%) abiotic Cr-Fe component in the fits of pellet 4 probably appeared due to the abiotic reduction of Cr(VI) by excess Fe(II). The effect of excess Fe(II) was more noticeable in the abiotic reduction samples (Fig. 1). The spectra of the sample with high Fe (Cr:Fe, 1:40) had a more definitive shoulder structure than the spectra of the samples with low F (Cr:Fe, 1:2.7 and 1:5); one possibility that could explain the spectral differences is that the former was more crystalline.

The rate of abiotic reaction of Cr(VI) with Fe(II) depends on the ratio of Fe(II):Fe(III) but typically follows first-order kinetics with a pH-dependent rate constant (Buerge and Hug, 1997; Sedlak and Chan, 1997). The rate of reduction can be accelerated by the presence of mineral surfaces (Buerge and Hug, 1999) and decreased by the presence of Fe(II)-stabilizing organic ligands (Buerge and Hug, 1998).

Environmental Implications of Findings

These results are environmentally relevant because the structure of the products of bioremediation will affect their long-term stability and potential for remobilization. The Cr(III) products due to Cr(VI) reduction by biogenic Fe(II) were clearly different from pure $Cr(OH)_3$ or an entire compositional series of laboratory-synthesized abiotic Cr-Fe (hydr)oxides [$Cr_xFe_{1-x}(OH)_3$]. This is the first important result because it makes clear that studies of the reoxidation potential of Cr(III) materials resulting from bioreduction should examine biogenic Cr(III) materials in addition to the common abiotically synthesized $Cr_xFe_{1-x}(OH)_3$. Our results also show that environmentally relevant changes in the precipitation environment, such as the presence of cell surfaces or excess organic carbon and available Fe(II) concentrations, can affect the structure of Cr-Fe (hydr)oxides. The solubility and reoxidation potential of the new phases cannot be determined directly from structural information in the XANES spectra, and further research is needed to evaluate their long-term stability in similar systems. However, several possibilities can be discussed. First, it has been shown that the abiotic $Cr_xFe_{1-x}(OH)_3$ have generally lower solubility than pure Cr phases (Sass and Rai, 1987), which is likely to affect the rate of Cr(III) reoxidation by limiting the steady-state aqueous concentration of Cr(III). In addition, the possibility that the column solids are coprecipitated with or in close proximity to organic carbon in the form of cell structures or exudates could decrease the likelihood of reoxidation by maintaining the local redox potential to be low enough to remain within the stability field of Cr(III) rather Cr(VI) and/or providing readily available reducing agents for any Cr(VI) reappearing in the system. The presence of organic ligands will also affect the surface reactivity of the Cr-Fe (hydr)oxides, potentially blocking reactive surface sites. In contrast, smaller particles would have a greater potential for transport with advecting fluids, although no evidence for this was observed in our studies.

Summary and Conclusions

This study used spectroscopy and X-ray scattering techniques to examine the structure of reduced Cr precipitates in flow-through columns with different biogeochemical conditions. The distribution of chromium changes from primary minerals in the untreated sediments to less ordered secondary phases that were structurally similar across all the treated columns, irrespective of the predominant biogeochemical conditions. The reduced Cr phases were mixed-phase Cr(III)-Fe(III) (hydr)oxides that did not resemble the typically expected products of abiotic Cr(VI) reduction with dissolved Fe(II).

The spectroscopic data suggest that the main mechanism resulting in the formation of the secondary Cr-Fe minerals in the flow-through columns is a coupled biotic–abiotic reduction [i.e., biotic reduction of Fe(III) to Fe(II) followed by abiotic reduction of Cr(VI) by the Fe(II)]. Furthermore, a comparison of laboratory-synthesized samples showed that the structure of even purely abiotic Cr(VI) reduction by Fe(II) can be affected by other factors, such as excess Fe(II) in solution or the presence of cellular matter. These findings are important from a remediation perspective because the solubility and

reoxidation potential of the reduced Cr phases produced under realistic subsurface conditions depends on their final structure.

Acknowledgments

References

1. ↵

   Arias, Y.M., and B.M. Tebo. 2003. Cr(VI) reduction by sulfidogenic and nonsulfidogenic microbial consortia. Appl. Environ. Microbiol. 69(3):1847–1853. doi:10.1128/AEM.69.3.1847-1853.2003**[View Article]**

2. ↵

   Beauchemin, S., D. Hesterberg, and M. Beauchemin. 2002. Principal component analysis approach for modeling sulfur K-XANES spectra of humic acids. Soil Sci. Soc. Am. J.66:83–91. doi:10.2136/sssaj2002.0083**[View Article]**

3. ↵

   Beller, H.R., R. Han, U. Karaoz, H. Lim, and E.L. Brodie. 2013. Genomic and physiological characterization of the chromate-reducing, aquifer-derived firmicute Pelosinus sp. strain HCF1. Appl. Environ. Microbiol. 79(1):63–73. doi:10.1128/AEM.02496-12**[View Article]**

4. ↵

   Beller, H.R., L. Yang, C. Varadharajan, R. Han, H.C. Lim, U. Karaoz, and P.S. Nico.2014. Divergent aquifer biogeochemical systems converge on similar and unexpected Cr(VI) reduction products. Environ. Sci. Technol. 48:10699–10706.doi:10.1021/es5016982**[View Article]**

5. ↵

   Buerge, I.J., and S.J. Hug. 1997. Kinetics and pH dependence of chromium(VI) reduction by iron(II). Environ. Sci. Technol. 31(5):1426–1432. doi:10.1021/es960672i**[View Article]**

6. ↵

   Buerge, I.J., and S.J. Hug. 1998. Influence of organic ligands on chromium(VI) reduction by iron(II). Environ. Sci. Technol. 32(14):2092–2099. doi:10.1021/es970932b**[View Article]**

7. ↵

   Buerge, I.J., and S.J. Hug. 1999. Influence of mineral surfaces on chromium(VI) reduction by iron(II). Environ. Sci. Technol. 33(23):4285–4291. doi:10.1021/es981297s**[View Article]**

8. ↵

   Chupas, P.J., X. Qiu, J.C. Hanson, P.L. Lee, C.P. Grey, and S.J.L. Billinge. 2003.Rapid-acquisition pair distribution function (RA-PDF) analysis. J. Appl. Cryst. 36(6):1342–1347. doi:10.1107/S0021889803017564**[View Article]**

9. ↵

   Cornell, R., and U. Schwertmann. 2003. The iron oxides: Structure, properties, reactions, occurrences and uses. 2nd ed. Wiley-VCH, Weinheim, Germany. doi:10.1002/3527602097

10. ↵

Dai, R., J. Liu, C. Yu, R. Sun, Y. Lan, and J.-D. Mao. 2009. A comparative study of oxidation of Cr(III) in aqueous ions, complex ions and insoluble compounds by manganese-bearing mineral (birnessite). Chemosphere 76(4):536–541.doi:10.1016/j.chemosphere.2009.03.009**[View Article]**

11. ↵

Dove, P.M., de Yoreo, J.J., and Weiner, S. , editors. 2003. Biomineralization: Reviews in mineralogy and geochemistry. Vol. 54. Mineralogical Society of America, Chantilly, VA.

12. ↵

Eary, L.E., and D. Rai. 1988. Chromate removal from aqueous wastes by reduction with ferrous ion. Environ. Sci. Technol. 22(8):972–977. doi:10.1021/es00173a018**[View Article]**

13. ↵

Fendorf, S.E., and G. Li. 1996. Kinetics of chromate reduction by ferrous iron. Environ. Sci. Technol. 30(5):1614–1617. doi:10.1021/es950618m**[View Article]**

14. ↵

Gräfe, M., E. Donner, R.N. Collins, and E. Lombi. 2014. Speciation of metal(loid)s in environmental samples by X-ray absorption spectroscopy: A critical review. Analytica Chimica Acta 822:1–22. **http://dx.doi.org/10.1016/j.aca.2014.02.044[View Article]**

15. ↵

A.P. Hammersley 1998. FIT2D V9.129 reference manual V3.1. ESRF Internal Report ESRF98HA01T. ESRF, Grenoble, France.

16. ↵

Han, R., J.T. Geller, L. Yang, E.L. Brodie, R. Chakraborty, J.T. Larsen, and H.R. Beller.2010. Physiological and transcriptional studies of Cr(VI) reduction under aerobic and denitrifying conditions by an aquifer-derived pseudomonad. Environ. Sci. Technol.44(19):7491–7497. doi:10.1021/es101152r**[View Article]**

17. ↵

Hansel, C.M., B.W. Wielinga, and S. Fendorf. 2003. Structural and compositional evolution of Cr/Fe solids after indirect chromate reduction by dissimilatory iron-reducing bacteria. Geochim. Cosmochim. Acta 67(3):401–412. doi:10.1016/S0016-7037(02)01081-5**[View Article]**

18. ↵

Jardine, P.M., S.E. Fendorf, M.A. Mayes, I.L. Larsen, S.C. Brooks, and W.B. Bailey.1999. Fate and transport of hexavalent chromium in undisturbed heterogeneous soil.Environ. Sci. Technol. 33(17):2939–2944. doi:10.1021/es981211v**[View Article]**

19. ↵

Lovley, D.R., and E.J.P. Phillips. 1987. Rapid assay for microbially reducible ferric iron in aquatic sediments. Appl. Environ. Microbiol. 53(7):1536–1540.

20. ↵

E.R. Malinowski 2002. Factor analysis in chemistry. 3rd ed. John Wiley & Sons, Ltd., New York.

21. ↵

Manning, B.A., J.R. Kiser, H. Kwon, and S.R. Kanel. 2007. Spectroscopic investigation of Cr(III)- and Cr(VI)-treated nanoscale zerovalent iron. Environ. Sci. Technol. 41(2):586–592. doi:10.1021/es061721m**[View Article]**

22. ↵

Neal, A.L., K. Lowe, T.L. Daulton, J. Jones-Meehan, and B.J. Little. 2002. Oxidation state of chromium associated with cell surfaces of Shewanella oneidensis during chromate reduction. Appl. Surf. Sci. 202:150–159. doi:10.1016/S0169-4332(02)00550-0**[View Article]**

23. ↵

Palmer, C.D., and P.R. Wittbrodt. 1991. Processes affecting the remediation of chromium-contaminated sites. Environ. Health Perspect. 92:25–40.doi:10.1289/ehp.919225**[View Article]**

24. ↵

Patterson, R.R., S. Fendorf, and M. Fendorf. 1997. Reduction of hexavalent chromium by amorphous iron sulfide. Environ. Sci. Technol. 31(7):2039–2044.doi:10.1021/es960836v**[View Article]**

25. ↵

Puzon, G.J., A.G. Roberts, D.M. Kramer, and L. Xun. 2005. Formation of soluble organo–chromium(III) complexes after chromate reduction in the presence of cellular organics. Environ. Sci. Technol. 39(8):2811–2817. doi:10.1021/es048967g**[View Article]**

26. ↵

Qiu, X., J.W. Thompson, and S.J.L. Billinge. 2004. PDFgetX2: A GUI-driven program to obtain the pair distribution function from X-ray powder diffraction data. J. Appl. Cryst.37(4):678.. doi:10.1107/S0021889804011744**[View Article]**

27. ↵

R Core Team. R: A language and environment for statistical computing. R Foundation for Statistical Computing: Vienna, Austria, 2013.

28. ↵

Ravel, B., and M. Newville. 2005. ATHENA, ARTEMIS, HEPHAESTUS: Data analysis for X-ray absorption spectroscopy using \it IFEFFIT. J. Synchrotron Radiat. 12(4):537–541.doi:10.1107/S0909049505012719**[View Article]**

29. ↵

Sass, B.M., and D. Rai. 1987. Solubility of amorphous chromium(III)-iron(III) hydroxide solid solutions. Inorg. Chem. 26(14):2228–2232. doi:10.1021/ic00261a013**[View Article]**

30. ↵

Sedlak, D.L., and P.G. Chan. 1997. Reduction of hexavalent chromium by ferrous iron.Geochim. Cosmochim. Acta 61(11):2185–2192. doi:10.1016/S0016-7037(97)00077-X**[View Article]**

31. ↵

L.L. Stookey 1970. Ferrozine: a new spectrophotometric reagent for iron. Anal. Chem.42(7):779–781. doi:10.1021/ac60289a016**[View Article]**

32. ↵

Tang, Y., F.M. Michel, L. Zhang, R. Harrington, J.B. Parise, and R.J. Reeder. 2010.Structural properties of the Cr(III)-Fe(III) (oxy)hydroxide compositional series: Insights for a nanomaterial "solid solution." Chem. Mater. 22:3589–3598.**http://dx.doi.org/10.1021/cm1000472[View Article]**

33. ↵

S.M. Webb 2005. SIXpack: A graphical user interface for XAS analysis using IFEFFIT.Phys. Scr. 2005(T115):1011.. doi:10.1238/Physica.Topical.115a01011

34. ↵

Werner, M., P. Nico, B. Guo, I. Kennedy, and C. Anastasio. 2006. Laboratory study of simulated atmospheric transformations of chromium in ultrafine combustion aerosol particles.Aerosol Sci. Technol. 40(7):545–556. doi:10.1080/02786820600714353**[View Article]**

35. ↵

Whittleston, R.A., D.I. Stewart, R.J.G. Mortimer, Z.C. Tilt, A.P. Brown, K. Geraki, and I.T. Burke. 2011. Chromate reduction in Fe(II)-containing soil affected by hyperalkaline leachate from chromite ore processing residue. J. Hazard. Mater. 194(0):15–23.doi:10.1016/j.jhazmat.2011.07.067**[View Article]**

36. ↵

Wielinga, B., M.M. Mizuba, C.M. Hansel, and S. Fendorf. 2001. Iron promoted reduction of chromate by dissimilatory iron-reducing bacteria. Environ. Sci. Technol. 35(3):522–527.doi:10.1021/es001457b**[View Article]**